Tuning ubiquinone position in biomimetic monolayer membranes

Javier Hoyo[1*], *Ester Guaus*[1], *Juan Torrent-Burgués*[1]

[1]*Universitat Politècnica de Catalunya, Dpt. Chemical Engineering, 08222 Terrassa (Barcelona), Spain*

*Corresponding autor: javier.hoyo@upc.edu, C/ Colom 1, E-08222 Terrassa (Barcelona), Spain, Tlf: +34 937398043.

Abstract

Artificial lipid bilayers have been extensively studied as models that mimic natural membranes (biomimetic membranes). Several attempts of biomimetic membranes inserting ubiquinone (UQ) have been performed to enlighten which the position of UQ in the lipid layer is, although obtaining contradictory results. In this work, pure components (DPPC and UQ) and DPPC:UQ mixtures have been studied using surface pressure-area isotherms and Langmuir-Blodgett (LB) films of the same compounds have been transferred onto solid substrates being topographically characterized on mica using atomic force microscopy and electrochemically on indium tin oxide slides.

DPPC:UQ mixtures present less solid-like physical state than pure DPPC indicating a higher order degree for the later. UQ influences considerably DPPC during the fluid state, but it is mainly expelled after the phase transition at ≈ 26 $mN \cdot m^{-1}$ for the 5:1 ratio and at ≈ 21 $mN \cdot m^{-1}$ for lower UQ content. The thermodynamic studies confirm the stability of the DPPC:UQ mixtures before that event, although presenting a non-ideal behaviour. The results indicate that UQ position can be tuned by means of the surface pressure applied to obtain LB films and the UQ initial content. The UQ positions in the biomimetic membrane are distinguished by their formal potential: UQ located in "diving" position with the UQ placed in the DPPC matrix in direct contact with the electrode surface (-0.04 ± 0.02 V), inserted between lipid chains without contact to the substrate (0.00 ± 0.01 V) and parallel above the lipid chains (0.09 ± 0.02 V).

Keywords

Biomimetic membrane, dipalmitoylphosphatidylcholine, ubiquinone, modified ITO electrode, Langmuir-Blodgett film, electron transfer.

Abbreviations

AFM	Atomic Force Microscopy
CV	Cyclic voltammogram
DPPC	Dipalmitoylphosphatidylcholine
HPT	Head plus part of the tail
ITO	Indium-tin oxide
LB	Langmuir-Blodgett
LC	Liquid Condensed state
LE	Liquid Expanded state
LPT	Last part of the tail
MGDG	Monogalactosyldiacylglycerol
UQ	Ubiquinone

Highlights

Biomimetic films of dipalmitoylphosphatidylcholine (DPPC) inserting ubiquinone (UQ) have been built

DPPC:UQ mixtures present less solid-like state than pure DPPC due to UQ influence

UQ presents two main positions in the lipid matrix: diving and swimming

The different UQ positions lead to three different redox processes

UQ positions are tuned by the UQ initial content, surface pressure and lipid nature

1. Introduction

Artificial lipid layers are considered biomimetic membranes owing to they are stable, robust and maintain good fluidity and lateral mobility [1]. The composition of biomimetic membranes is tuneable including the insertion of proteins, nanoparticles and other species within the membrane or at its surface [2, 3]. Biomimetic membranes have been used for several purposes such as biotechnological nanodevices [4, 5], membrane structure characterization [6, 7], study of the structure of membrane-associated proteins [8], membrane-drug interaction [9–11] and peptide-lipid interactions [12, 13].

Dipalmitoylphosphatidylcholine (DPPC) is a phospholipid consisting of two saturated dipalmitoyl chains and a choline headgroup (Fig. 1a). The headgroup is zwitterionic so it should be uncharged at neutral pH but it is slightly negative charged in solution due to the orientation of the headgroup around the headgroup|water interface [14]. Ubiquinone-10 (UQ) (Fig. 1b) act as a proton and electron transporter in the respiratory chain of the inner mitochondrial membranes [11, 15]. The system DPPC:UQ has been chosen to study the position of UQ mimicking the mitochondrial membrane based on the high phosphatidylcholine content on this membrane [16].

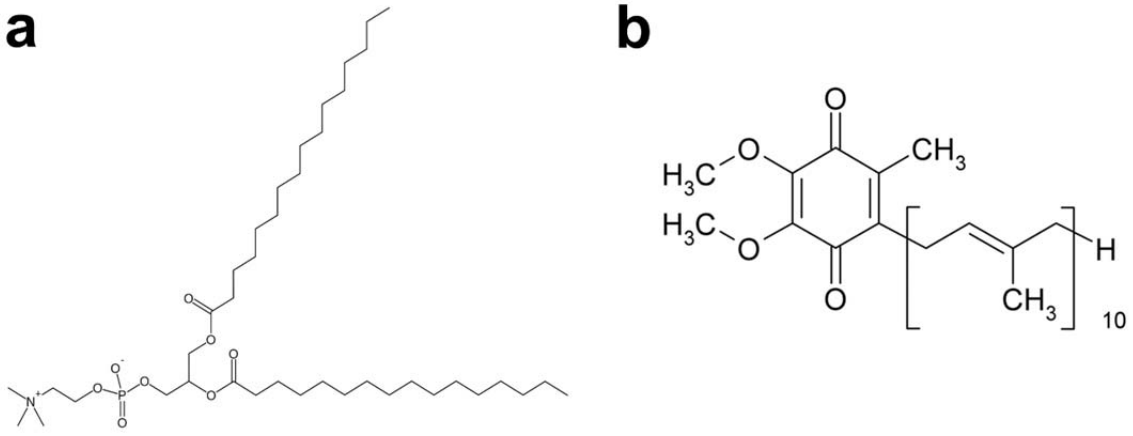

Fig. 1 Scheme of a molecule of (a) DPPC and (b) UQ.

The position of UQ in natural membranes has been subject of study although obtaining contradictory results. Two main positions are described in the literature: “diving quinone” and “swimming quinone” [17].

Diving quinone presents an inflexion point in the hydrocarbon tail of the UQ, which separates the UQ molecules in the head plus part of the tail (HPT) and the last part of the tail (LPT). HPT is placed in parallel to the lipid chains, inserted between them whereas LPT is free to move. Dynamic simulations of the system [17] and the results of Aranda and Gomez-Fernandez [18] suggest that the UQ headgroup is placed between the 3rd and the 6th carbon atom of the lipid chain counted from the carbonyl carbon. The position corresponding to diving quinone has been proposed using several biomimetic systems and techniques such as differential scanning calorimetry (DSC) [18, 19], wide angle X-ray diffraction analysis [19], difference infrared-spectroscopy [20], fluorescence anisotropy [21], fluorescence quenching [22], NMR chemical shift-polarity correlation [23, 24], linear dichroism [25], surface-pressure isotherms [26, 27], surface-enhanced infrared adsorption spectroscopy [28, 29] and voltammetric techniques [30].

UQ in swimming position has free movement on the bilayer midplane, being its head buried less than 1 nm in the lipid chains of both leaflets of the bilayer [17]. The swimming position of UQ is more stable and confers higher lateral diffusion [31, 32] than the diving position, which is explained by the fact that the hydrophobic interactions between lipid chains are not disturbed by the presence of UQ besides the lower viscosity of the hydrocarbon tails in the midplain compared to the polar head region [33, 34]. The “swimming” position has been confirmed using several techniques like fluorescence quenching [35], voltammetric techniques [30, 36], performing surface-pressure isotherms [22, 26, 27], nuclear magnetic resonance [22, 37–42], differential infrared spectroscopy [21], DSC [18, 20, 43, 44], neutron diffraction [45], surface-enhanced infrared adsorption spectroscopy [28] and linear dicroism [25].

The use of Langmuir and Langmuir-Blodgett (LB) techniques allows a higher control on the membrane physical state and structure compared with vesicle fusion technique [46, 47]. The physical states derived from the surface-pressure isotherms are confirmed by the zones with different height observed in AFM images, which confirms the presence of UQ in both physical states. Electrochemistry allows the study of the redox behaviour of UQ immobilized

on the DPPC matrix. The presence of redox peaks at different potential indicates that UQ is present in different environments that are correlated with different UQ positions in the membrane. Therefore, we enlighten the position of UQ in a biomimetic membrane of DPPC and the conditions that lead to each position, thus we can tune this position on demand being useful in biosensors applications and routed electron transfer. The present article complement our first study [30] with the DPPC:UQ system, focused on its electrochemical behaviour for artificial photosynthesis on ITO. The current text revise the results obtained, extending the π-A isotherms, AFM and electrochemical results to describe in deep the whole DPPC-UQ interactions, physical states and UQ position. These interactions are compared with those of the monogalactosyldiacylglycerol (MGDG) - the principal lipid component of thylakoid membranes- with UQ and the differences based on the lipid nature are discussed.

2. Materials and methods

2.1 Materials

UQ HPLC grade was provided by Sigma-Aldrich and DPPC was purchased from Avanti Polar Lipids. KH_2PO_4, KCl and chloroform of analytical grade from Sigma-Aldrich were used in solutions preparation. Water was ultrapure MilliQ® (18.2 MΩ·cm). Mica sheets were purchased from TED PELLA Inc (CA) and ITO (15 Ω/sq) deposited on glass slides of (10 mm x 25 mm) were purchased to SOLEMS (France).

2.2 Methods

2.2.1 Monolayer formation

Langmuir and Langmuir-Blodgett monolayer formation were carried on a trough (Nima Technology, Cambridge, UK) model 1232D1D2 equipped with two movable barriers as described in [48]. Briefly, the trough was cleaned twice with chloroform and once with MilliQ quality water previously to the subphase (MilliQ water) addition. Solutions of DPPC, UQ and DPPC:UQ were prepared using chloroform and spread at the air|liquid interface using a high precision Hamilton microsyringe. Barrier closing rates were fixed at 50 $cm^2 \cdot min^{-1}$ (6.3 $Å^2 \cdot molec^{-1} \cdot min^{-1}$) for isotherm registration and at 25 $cm^2 \cdot min^{-1}$ (3.1 $Å^2 \cdot molec^{-1} \cdot min^{-1}$) for LB film transfer. LB film transfer at defined surface pressure values was conducted dipping (5 mm/min) the freshly cleaved mica or freshly cleaned ITO through the air|liquid interface on

the subphase before adding the solution. Experiments were conducted at 21±1ºC and repeated a minimum of three times for reproducibility control.

2.2.2 AFM characterization

AFM topographic images of LB films were acquired in air tapping mode using a Multimode AFM controlled by Nanoscope IV electronics (Veeco, Santa Barbara, CA) under ambient conditions. Triangular AFM probes with silicon nitride cantilevers and silicon tips were used (SNL-10, Bruker), which have a nominal spring constant ≈ 0.35 $N \cdot m^{-1}$. Data obtained was processed using Nanoscope Analysis 1.4 software using the flatten filter, the section application and the bearing analysis for coverage area.

2.2.3 Electrochemical characterization

Voltammetric measurements were performed in a conventional three-electrode cell using an Autolab Potentiostat-Galvanostat PGSTAT-12 (Ecochemie, NL). Working electrodes were freshly-cleaned ITO slides cleaned once with ethanol and three times with MilliQ grade water. Counter electrode was a platinum wire in spiral geometry and the reference electrode was an Ag/AgCl/3M KCl microelectrode (DRIREF-2SH, World Precision Instruments). All reported potentials are referred to this electrode. The electrochemical cell contained 0.150 M KCl as supporting electrolyte at pH 7.4 adjusted with the 0.100 M KH_2PO_4/K_2HPO_4 buffer solution. All solutions were freshly prepared with MilliQ grade water de-aerated with a flow of Ar gas for 15 min prior to the cyclic voltammetry experiments, which were conducted at 21 ± 1ºC. Voltammetric experiments were carried out at several scan rates, scanning towards cathodic potentials in a homemade glass cell with a reaction area of 33 mm^2.

3 Results and Discussion

3.1 π-A isotherms, physical states and mixing behaviour

π-A isotherms of DPPC, UQ and their mixtures at biological relevant ratios referred to the mean area per molecule are presented in Fig. 2, being the most significant values summarized in Table 1. The inverse of the compressibility modulus (C_s^{-1}) -Inset of Fig. 2- provides information about the elasticity and the compressibility of the corresponding monolayer and is used for physical state identification. C_s^{-1} is obtained from the described π-A isotherms

calculated according to Expression 1, where A is the mean area per molecule (in $Å^2 \cdot molecule^{-1}$), π the surface pressure (in $mN \cdot m^{-1}$) and T the absolute temperature (in K).

$$C_s^{-1} = -A\left(\frac{d\pi}{dA}\right)_T \qquad \text{Expression 1}$$

Each C_s^{-1} curve (inset Fig. 2) presents three local minimum points -kink points- and the isotherms of Fig. 2 can be divided into two zones according to the second kink point, present at ≈ 26 $mN \cdot m^{-1}$ for the 5:1 ratio and at ≈ 21 $mN \cdot m^{-1}$ for the 10:1 and 20:1 ratios. The disturbing effect of UQ molecules in the DPPC matrix is observed in the area per molecule of the isotherms below the second kink point, where this area increases as UQ content in the DPPC:UQ mixture is enlarged. The presence of UQ in the initial zone impedes the packing of DPPC headgroups, and therefore, the hydrophobic interactions between the DPPC chains are also reduced, as it was seen for UQ inserted in phospholipids [49]. This phenomena was also observed by Bilewicz et al. [50] using UQ and $C_{18}SH/C_{18}OH$ and by Kruk et al. [51] using PQ and unsaturated MGDG mixtures.

Above the surface pressure of the second kink point, most of the UQ molecules have been expelled, as it will be explained. In addition, all the π-A isotherms of the mixtures have a similar slope, showing also a similar area per molecule. On the other hand, the different slope of the π-A isotherms of the mixtures compared with that of pure DPPC indicates that part of UQ molecules are still remaining in the DPPC matrix, although it seems to be in low content.

The C_s^{-1} curves of DPPC:UQ mixtures (inset of Fig. 2) present similar shape with differences according to the UQ content around the kink points. DPPC shows phase transition from liquid expanded (LE) to liquid condensed (LC) [52] at ≈ 6 $mN \cdot m^{-1}$ whereas for DPPC:UQ mixtures it depends on the UQ content. The first kink point, at ≈ 18 $mN \cdot m^{-1}$ for the 5:1 ratio and at ≈ 8 $mN \cdot m^{-1}$ for the 10:1 and 20:1 ratios, suggests an increase of the DPPC molecules ordering, which implies the beginning of a progressive expulsion of the UQ molecules from the matrix owing to steric hindrances. The second kink point indicates the phase transition from LE to LC of the DPPC molecules, which implies the expulsion of most of the remaining UQ molecules. Therefore, the compactness of the mixture monolayer is enhanced. The third kink point (placed at ≈ 44 $mN \cdot m^{-1}$) seems to represent a reorientation of the DPPC molecules, which implies the last stage of UQ molecules expulsion from the matrix.

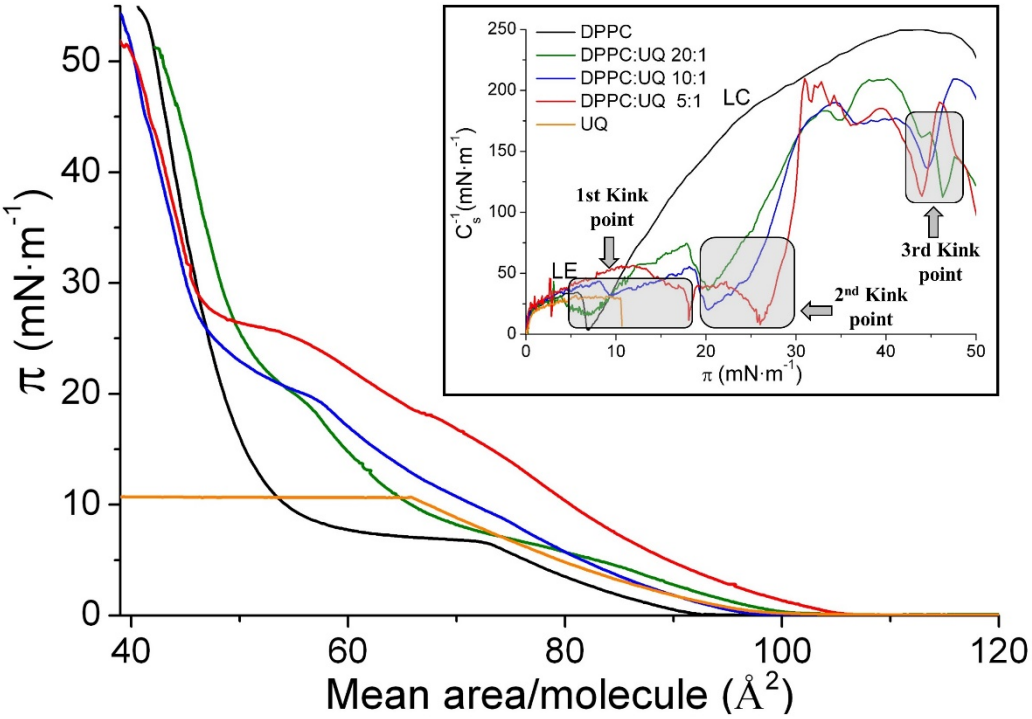

Fig. 2 π-A isotherms for DPPC, UQ and DPPC:UQ mixtures at 21 ± 1 ºC on water subphase. Inset: Inverse of the compressibility modulus vs. surface pressure corresponding to the described π-A isotherms.

Table 1. Collapse pressure, the second kink point position for DPPC, UQ and their biological mixtures obtained from Fig. 2. Second kink point is presented due to its correlation with physical state transition.

	Collapse pressure ($mN \cdot m^{-1}$)	2nd Kink point pressure ($mN \cdot m^{-1}$)	2nd Kink point area ($Å^2 \cdot molec^{-1}$)
DPPC	55	-	-
DPPC:UQ 20:1	52	21	55
DPPC:UQ 10:1	55	21	56
DPPC:UQ 5:1	52	26	52
UQ	11	-	-

Phase rule

The collapse pressure is ≈ 53 $mN \cdot m^{-1}$ for all DPPC and DPPC:UQ mixtures. In a two component monolayer, if components are completely immiscible, a lower collapse pressure of one of the components will be observed [53]. Maintaining temperature and external pressure constant, the number of degrees of freedom F of the monolayer system is given by the Expression 2 [54], where C_B is the number of components in the bulk, C_S is the number of components confined at the surface, P_B is the number of bulk phases, and P_S is the number of monolayer phases in equilibrium with each other.

$$F = C_B + C_S - P_B - P_S + 1 \qquad \text{Expression 2}$$

In our system, at the air|water interface, $C_B = 2$ (air and water), $C_S = 2$ (DPPC and UQ), and $P_B = 2$ (gas and liquid), thus $F = 3 - P_S$. According to our results, the collapse pressure is practically fixed, discarding experimental deviations, for pure DPPC and DPPC:UQ mixtures. This indicates zero degrees of freedom and therefore, following the previous reasoning, $P_S = 3$. Thus, at the collapse equilibrium of the mixtures isotherms coexist: DPPC (LC), DPPC (collapse) and expelled UQ.

Thermodynamic study

The representation of the mean area per molecule vs. the molar fraction at selected pressures gives idea about the ideality of the mixture (Expression 3). Where A^E is the excess area, A_{12} the mean area per molecule for the mixture, A_1 and A_2 the area per molecule for the individual components and, x_1 and x_2 the molar fraction of each component.

$$A^E = A_{12} - (x_1 A_1 + x_2 A_2) \qquad \text{Expression 3}$$

Moreover, the representation of the ΔG_{mix} vs. UQ molar fraction gives idea about the stability of the mixture (Expressions 3-6). Where G^E is the excess free energy of mixing, ΔG_{mix} the free energy of mixing, N_A is the Avogadro's number, R the gas constant and T the absolute temperature.

$$G^E = N_A \int_0^{\pi} A^E d\pi \qquad \text{Expression 4}$$

$$\Delta G_{mix} = \Delta G_{id} + G^E \qquad \text{Expression 5}$$

$$\Delta G_{id} = RT(x_1 \ln x_1 + x_2 \ln x_2) \qquad \text{Expression 6}$$

Fig. 3a plots the area per molecule vs. the UQ molar fraction of DPPC:UQ mixtures at several surface pressures before the main UQ expulsion at the second kink point. At a surface pressure above this event, the thermodynamic study has not been performed due to the UQ content in the DPPC:UQ matrix is unknown and significantly lower than the initial presence.

The positive deviations observed at $\pi \leq 20$ mN·m^{-1} (Fig. 3a) correlate that DPPC and UQ form non-ideal mixtures indicating that the interactions between components are weaker than the interactions between single components [2], thus facilitating the formation of enriched

domains [48, 53] at high UQ content. ΔG_{mix} vs. UQ molar content (Fig. 3b) presents negative values for ΔG_{mix} at $\pi \leq 10$ mN·m^{-1} indicating that mixed monolayers of DPPC:UQ are more stable than pure components [2]. At higher surface pressures, the mixed monolayer is not stable, which favours the UQ expulsion. The formation of non-ideal mixtures between DPPC and UQ at low surface pressure is anticipated based on the difference in the chain length between both molecules that favours the flip-flop movement of the UQ chain that protrudes DPPC molecules. Therefore, this movement disturbs the DPPC monolayer causing a molecular area increase [51, 55].

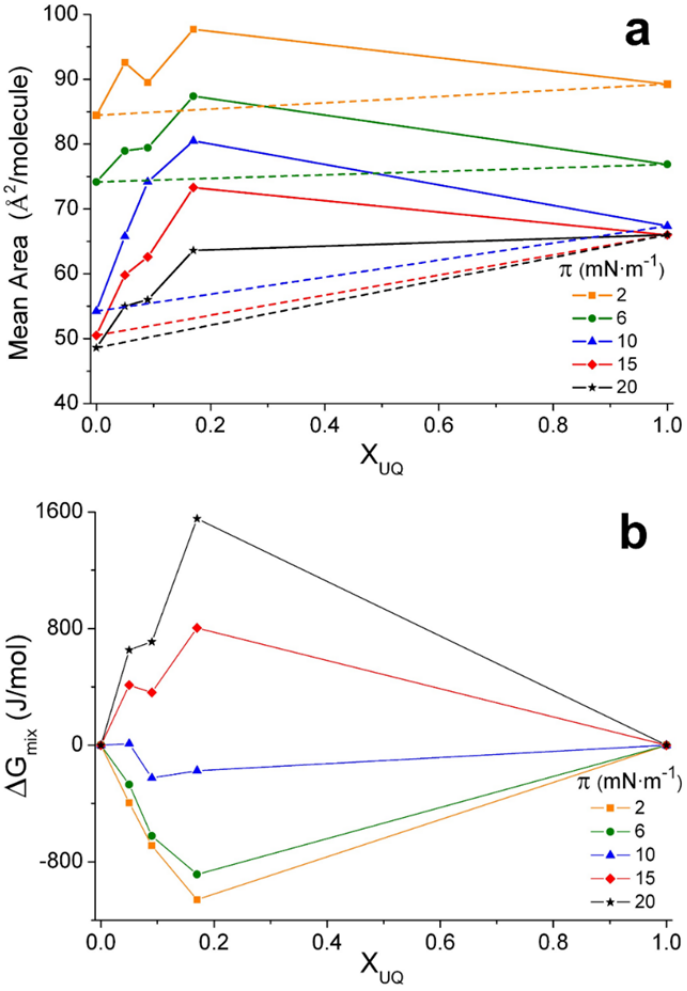

Fig. 3 a) Plot of mean area per molecule vs. molar fraction for DPPC, UQ and DPPC:UQ mixtures at several surface pressures before the main UQ expulsion. Discontinuous straight line represents the ideal behaviour for each surface pressure. b) Plot of the mixing energy vs. the molar fraction for DPPC, UQ and DPPC:UQ mixtures at several surface pressures before the main UQ expulsion.

3.2 AFM

Fig. 4 shows AFM topographic images corresponding to pure DPPC (images a-c) and DPPC:UQ 5:1 (images d-f) mixtures transferred on mica at several surface pressures, confirming that the presence of UQ (image 4d) has a strong influence on the DPPC matrix (image 4a).

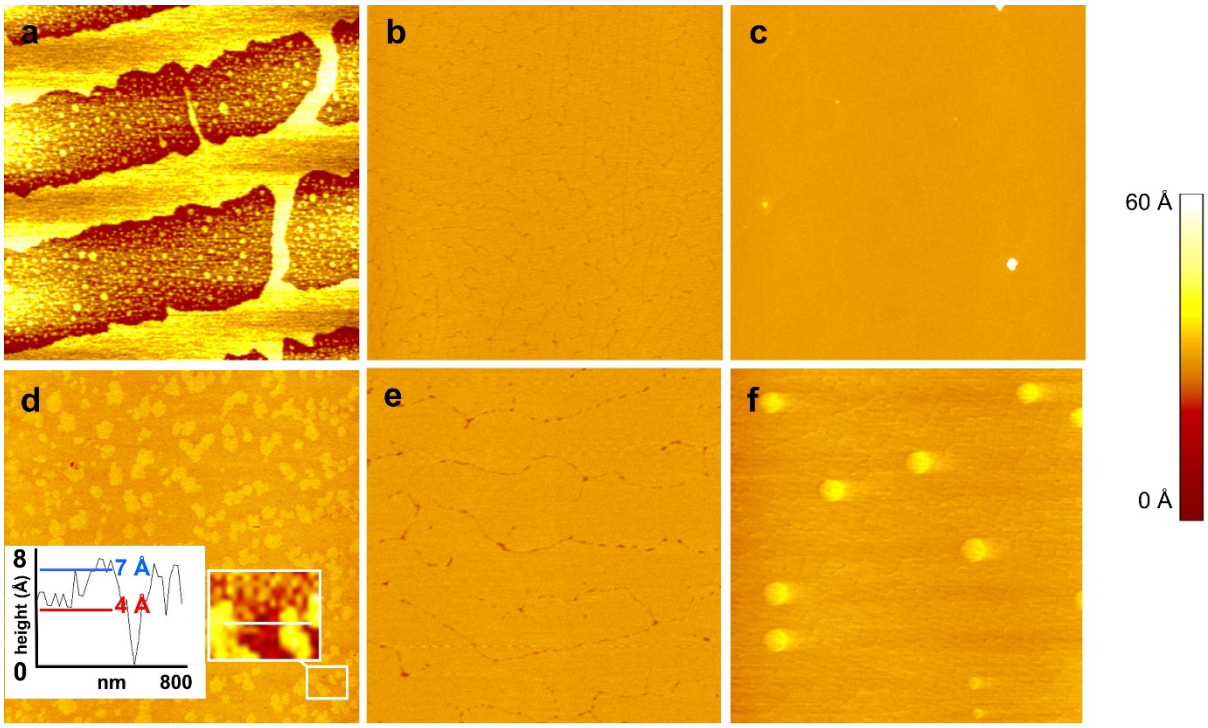

Fig. 4 AFM images (5µm x 5µm) for LB films of DPPC system transferred on mica at 21ºC at (a) $\pi = 6$ mN·m^{-1}, (b) $\pi = 25$ mN·m^{-1} and (c) $\pi = 40$ mN·m^{-1} and DPPC:UQ 5:1 at (d) $\pi = 6$ mN·m^{-1}, (e) $\pi = 25$ mN·m^{-1} and (f) $\pi = 40$ mN·m^{-1}.

DPPC on mica at $\pi = 6$ mN·m^{-1} (image 4a) forms a solid-like phase (fair zones) with a portion of fluid-like phase (dark zones) owing to stronger neighbour interactions of the lipid molecules. At $\pi = 25$ mN·m^{-1} the monolayer is solid-like state with short depth (< 1 Å) grooves that vanish at $\pi = 33$ mN·m^{-1}. DPPC:UQ 5:1 system at $\pi = 6$ mN·m^{-1} presents solid-like phase zones with a high portion of fluid-like phase zones. It is interesting to point out that this image, only for this high UQ content, presents small black zones (holes) that correspond to the mica surface (inset in image 4d).The compression leads to a more solid-like state of the ordered zones up to $\pi = 33$ mN·m^{-1} where the monolayer presents uniform phase with rounded shape protrusions of diameter 100 nm and 8 ± 2 Å height over it. AFM topographic images have been performed with the systems DPPC:UQ 10:1 and 20:1 (not shown) obtaining a behaviour comprised between pure DPPC and DPPC:UQ 5:1.

Considering the C_s^{-1} results (section 3.1) and the relative heights observed at each surface pressure permit obtaining the physical state corresponding to each shade [56], being dark zones corresponding to LE and fair zones to LC. DPPC and DPPC:UQ mixtures present grooves of depth < 4 Å at the LC phase, which suggest that the continuous phase has been formed by fusion of rigid domains.

The non-observation of uncovered mica zones -except for the explained case of DPPC:UQ 5:1 at π = 6 mN·m^{-1} - permits obtaining the proportion of each physical state at each surface pressure (Fig. 5). The surface covered by the solid-like state at each surface pressure increases quickly when increasing the surface pressure from π = 6 mN·m^{-1} (77%) up to the π = 25 mN·m^{-1} where this physical state covers the 100% of the available area. On the other hand, the DPPC:UQ systems show the expected trend of more surface covered by the solid-like state when decreasing the UQ content. Increasing the surface pressure, all the DPPC:UQ systems increase the presence of LC achieving at π = 25 mN·m^{-1} a nearly sustained increase, which is correlated with that the major content of UQ has been rejected from the lipid matrix. DPPC and DPPC:UQ mixtures present similar tendency of covered area by the solid-like state (fair shade in Fig. 4) although the height of the pure DPPC domains is higher, thus indicating that, once transferred, the interactions mica-DPPC or mica-DPPC:UQ are similar at low UQ content and the UQ presence mainly affects the DPPC molecules tilting.

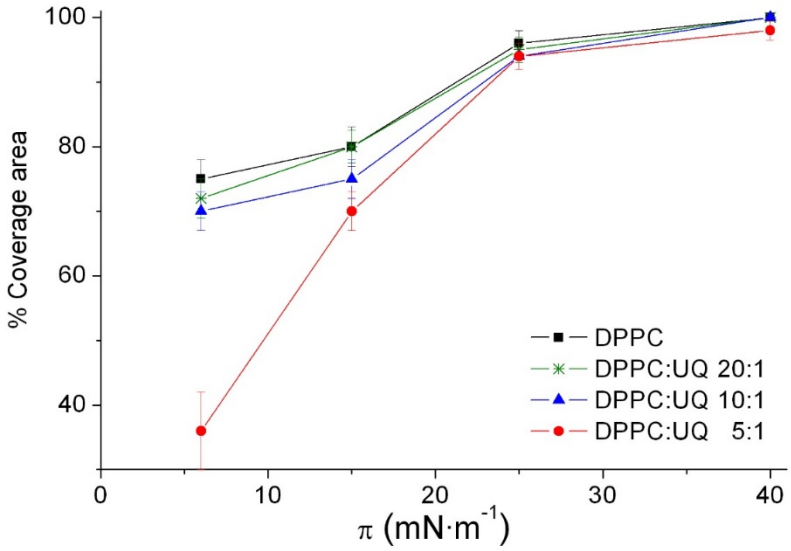

Fig. 5. Monolayer coverage of fair brown zones on mica surface for pure DPPC and DPPC:UQ mixtures, obtained from AFM images.

The simultaneous presence of two different physical states at each surface pressure for both the DPPC and DPPC:UQ systems indicates that both systems starts the LE to LC physical state transition at very low surface pressure. Pure DPPC system achieves the entire mica surface covered by the LC state at lower surface pressure than the DPPC:UQ systems (Fig. 5), which is explained by the presence of UQ in the DPPC:UQ mixtures, which impedes sterically the packing of the DPPC molecules. The size of the LC domains is reduced when increasing the UQ content in the DPPC:UQ mixture (not shown), which indicates that part of the UQ content is in the LC domains. The conclusions obtained using AFM are similar to those obtained using fluorescence microscopy [55].

3.3 Electrochemical behaviour

The electrochemical behaviour of the systems ITO-UQ and ITO-DPPC:UQ was studied in a previous article of our group [30] and the voltammograms are summarized in Fig. 6. UQ is surface confined in both systems, presenting pure UQ the formal potential of process I (E_f (I)) at -0.02 ± 0.02 V and that of process II (E_f (II)) at = 0.09 ± 0.02 V. The ITO-DPPC:UQ 5:1/electrolyte system at $\pi \leq 15$ mN·m^{-1} presents only one irreversible process (process I) based on its analogy with process I described for pure UQ. The ITO-DPPC:UQ 5:1/electrolyte system at $\pi = 25$ mN·m^{-1} shows a wide reduction peak, that draws three waves, and two wide oxidation peaks are observed. At $\pi = 40$ mN·m^{-1} three reduction peaks are clearly differentiated in the cathodic scan and two oxidation peaks in the anodic scan. The second oxidation peak that appear at $\pi = 25$ mN·m^{-1} and $\pi = 40$ mN·m^{-1} has been assigned as I_O'+II_O due to it represents the convolution of both contributions. The position of peak I_O' (E_f (I') = 0.00 ± 0.01 V) alone is observed in the DPPC:UQ 10:1 system owing to the process II is not present at low UQ content [30].

The non-symmetrical peak shape, which has also been observed previously for similar systems [57, 58], is explained by differences in the hydrophilic character of the redox couple UQ/UQH_2. UQH_2 presents higher polarity than the oxidized form (UQ) presenting more attractive interactions by dipole-dipole or hydrogen bond between UQH_2 and DPPC headgroups. Moreover, the interactions UQH_2-ITO, UQH_2-UQH_2 and UQH_2-water are also more favourable [26, 51, 57]. Second, the redox peaks separation (Fig. 7) for each process is larger than the expected for such systems. In addition, the separation for process I' is larger

than for process I indicating that process I' is even more irreversible than process I. Both processes increase their irreversibility as the scan rate is enhanced. A similar trend can be inferred for process II – only observed for the ITO-DPPC:UQ 5:1/electrolyte system (not shown) - and both are explained by the slow charge transfer rates at the ITO-monolayer|electrolyte interface [57]. In addition, the increase in the scan rate affects in a larger extent the oxidation peak potential than the reduction one (Fig. 7), which produces that the midpoint potential for process I and I' has scan rate dependence, confirming the higher stability of the reduced form (UQH_2) in the polar region.

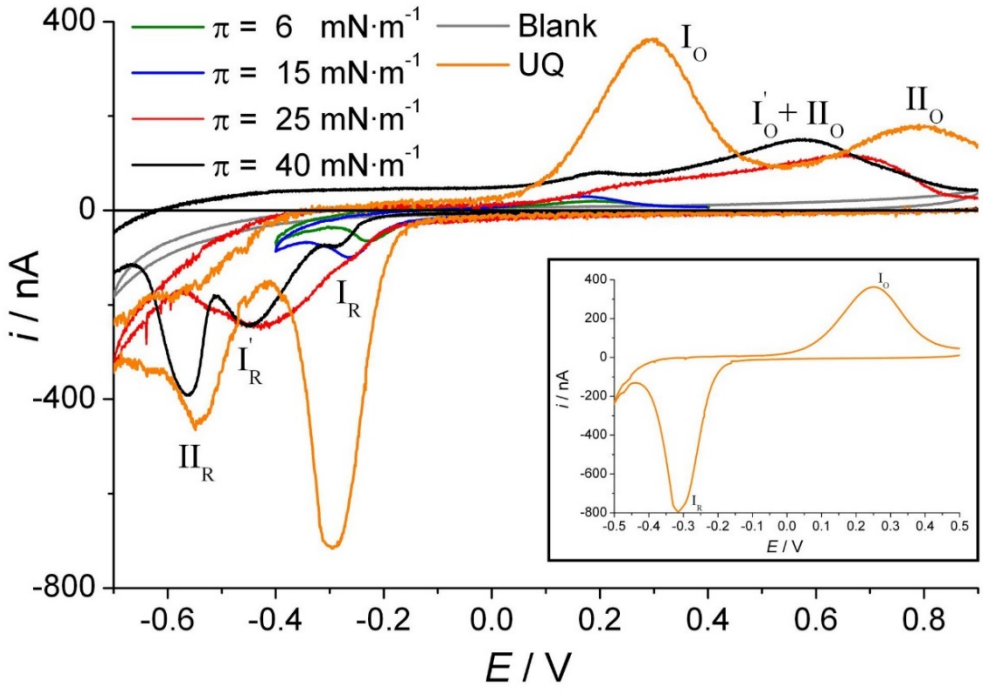

Fig. 6 Cyclic voltammograms of ITO-UQ LB film transferred at π = 11 mN·m^{-1} and ITO-DPPC:UQ 5:1 LB films transferred at several surface pressures. Blank line represents CV of the ITO-DPPC electrode at π = 40 mN·m^{-1}. Inset shows the cyclic voltammogram of ITO-UQ LB film transferred at π = 11 mN·m^{-1} and scanned in a short potential window. All CVs have been performed using 0.150 M of KCl electrochemical cell using potassium phosphate buffered solution at pH 7.4 and at a scan rate of 10 mV·s^{-1}.

Based on the results of the performed techniques, process II involves the UQ molecules that have been expelled from the DPPC matrix and are confined on top of the monolayer. Process I describes the behaviour of UQ molecules in direct contact with the ITO electrode. Finally, process I' presents a formal potential placed between that of processes I and II that permits assigning process I' to an intermediate position [30, 59] where the UQ head is buried near the DPPC molecules heads without contact to the substrate.

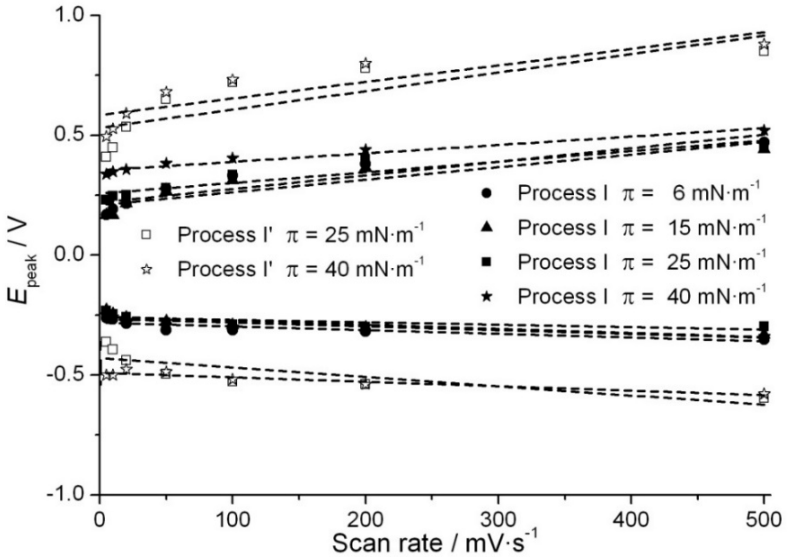

Fig. 7 Peak potential vs. scan rate for the ITO-DPPC:UQ 10:1/electrolyte system transferred at several surface pressures.

At low initial UQ content, the swimming position is not favoured due to the fast ordering of the LE to LC state favours the diving position without ITO-UQ contact. The ITO-DPPC:UQ/electrolyte 5:1 presents an exceeding UQ content that at high surface pressures is not able to be placed in position I and I'. Thus, these exceeding molecules are expelled to the top of the monolayer where the hydrophilicity of the medium added to the hydrophobicity of the end part of the DPPC chains stabilize the swimming position [55], avoiding the steric disturbing of being inserted between the DPPC chains.

UQ position in biomimetic membranes based on different lipids

This work concludes that the ordering process of pure DPPC molecules leads the DPPC:UQ monolayer ordering, thus expelling UQ molecules when the steric hindrances are high. Pure DPPC presents a moderated rate of phase change and induces to the DPPC:UQ systems a similar rate. Therefore, UQ is able to be present simultaneously in the three positions (diving with and without ITO-UQ contact, and swimming) and they can be tuned based on the transfer surface pressure and the initial UQ content. Conversely, UQ inserted in a biomimetic membrane of MGDG [3] presents maximum two positions. Pure MGDG presents a fast rate of phase transition and achieves solid-like structures with higher compactness. These properties are induced to MGDG:UQ systems leading MGDG to reject UQ both vertically -to

the top of the monolayer- and horizontally -to the fluid-like zones-, thus favouring the swimming position. Moreover, the UQ position is highly dependent on the lipid nature, the physical states that it presents upon compressing and the rate of the phase state change. In light of the results, the UQ position and the electron transfer direction can be anticipated by the physical states presented by the pure lipid and tuned on demand based on the lipid used for the monolayer and the initial UQ content.

4. Conclusions

DPPC monolayers present LE state before the phase transition to LC at $\pi \approx 6$ mN·m^{-1}. On the other hand, DPPC:UQ mixture monolayers present less solid-like physical states, owing to UQ influences considerably DPPC prior its main expulsion (second kink point) after the phase transition at ≈ 26 mN·m^{-1} for the 5:1 ratio and at ≈ 21 mN·m^{-1} for lower UQ content. The thermodynamic results indicate that DPPC and UQ mix and form stable, although non-ideal, mixtures prior the phase transition. The similar isotherm slope and the values of C_s^{-1} obtained for all the mixtures after the second inflexion point indicate that after the main UQ expulsion, a similar content of UQ remains for all compositions.

The interpretation of the results obtained from the different techniques enables elucidating the position of the UQ molecules in the phospholipid matrix. At low surface pressures, regardless the physical state of the DPPC:UQ domains, UQ is located in “diving” position with the UQ placed in the DPPC matrix in direct contact to the electrode surface (-0.04 ± 0.02 V) -process I- as can be inferred from electrochemical results comparing pure UQ and DPPC:UQ systems. The compression of the DPPC:UQ system implies the phase change from LE to LC of the remaining LE zones and the enhanced compactness of the LC zones, as can be inferred from the Langmuir monolayer and AFM results. Considering that the lateral rejection is hindranced, the vertical rejection of part of the UQ to the diving position without ITO-UQ contact, which correlates with redox process I’ (0.00 ± 0.01 V), is favoured. At high initial UQ content, part of the exceeding molecules are expulsed from the DPPC matrix obtaining the swimming position that is represented by the redox process II. At low initial UQ content, the swimming position is not favoured due to the moderated transition rate from LE to LC state favours entrapping UQ in diving position without ITO-UQ contact, as can be inferred from the non-presence of redox process II and the AFM results. The differences in the UQ

position observed in a biomimetic membrane of DPPC compared with that of MGDG [3] are explained by the higher compactness and faster LE-LC physical state change that the MGDG:UQ system presents.

The LB method permits a higher control of the UQ position compared to the vesicle preparation method. Therefore, the position of UQ in a lipid matrix may be anticipated by the physical states presented by pure lipid and tuned according to the initial UQ content and the surface pressure at which the LB film has been transferred, which favours the electron and proton transfer in the targeted direction.

Acknowledgements

The authors thank the economic support of the Spanish Government, through the project CTQ2007-68101-C02, and of the Catalonia Autonomic Government, through the project SGR2009-277. J Hoyo thanks to Universitat Politècnica de Catalunya its PhD grant. The authors declare that they have no conflict of interest.

Author contribution

All authors have equally contributed to the present article.

References

[1] Iglic A. *Advances in Planar Lipid Bilayers and Liposomes*. San Diego, California: Elsevier, 2011.

[2] Castellana ET, Cremer PS. Solid supported lipid bilayers: From biophysical studies to sensor design. *Surf Sci Rep* 2006; 61: 429–444.

[3] Hoyo J, Torrent-Burgués J, Guaus E. Biomimetic monolayer films of monogalactosyldiacylglycerol incorporating ubiquinone. *J Colloid Interf Sci* 2012; 384: 189–197.

[4] Fan Yin, Kafi AKM, Shin HK, et al. Human serum albumin-octadecylamine Langmuir-Blodgett film formed by spreading human serum albumin solution directly on subphase's interface covered with a layer of octadecylamine. *Thin Solid Films* 2005; 488: 223–229.

[5] Bally M, Bailey K, Sugihara K, et al. Liposome and lipid bilayer arrays towards biosensing applications. *Small* 2010; 6: 2481–2497.

[6] Schneider J, Dufrene YF, Barger WR, et al. Atomic Force Microscope Image Contrast Mechanisms on Supported Lipid Bilayers. *Biophys J* 2000; 79: 1107–1118.

[7] Oncins G, Picas L, Hernández-Borrell J, et al. Thermal response of Langmuir-Blodgett films of dipalmitoylphosphatidylcholine studied by atomic force microscopy and force spectroscopy. *Biophys J* 2007; 93: 2713–25.

[8] Merino-Montero S, Domènech Ò, Montero MT, et al. Preliminary atomic force microscopy study of two-dimensional crystals of lactose permease from Escherichia coli. *Biophys Chem* 2006; 119: 78–83.

[9] Leonenko Z V., Carnini A, Cramb DT. Supported planar bilayer formation by vesicle fusion: The interaction of phospholipid vesicles with surfaces and the effect of gramicidin on bilayer properties using atomic force microscopy. *Biochim Biophys Acta - Biomembr* 2000; 1509: 131–147.

[10] Leonenko Z V, Cramb DT. Revisiting lipid – general anesthetic interactions (I): Thinned domain formation in supported planar bilayers induced by halothane and ethanol. *Can J Chem* 2004; 82: 1128–1138.

[11] Ma W, Zhou H, Ying YL, et al. In situ spectroeletrochemistry and cytotoxic activities of natural ubiquinone analogues. *Tetrahedron* 2011; 67: 5990–6000.

[12] Vié V, Van Mau N, Chaloin L, et al. Detection of peptide-lipid interactions in mixed monolayers, using isotherms, atomic force microscopy, and fourier transform infrared analyses. *Biophys J* 2000; 78: 846–856.

[13] Takamoto DY, Lipp MM, von Nahmen A, et al. Interaction of lung surfactant proteins with anionic phospholipids. *Biophys J* 2001; 81: 153–169.

[14] Redondo-Morata L, Oncins G, Sanz F. Force spectroscopy reveals the effect of different ions in the nanomechanical behavior of phospholipid model membranes: The case of potassium cation. *Biophys J* 2012; 102: 66–74.

[15] Mitchell P. The protonmotive Q cycle: A general formulation. *FEBS Lett* 1975; 59: 137–139.

[16] Horvath SE, Daum G. Lipids of mitochondria. *Prog Lipid Res* 2013; 52: 590–614.

[17] Soderhall JA, Laaksonen A. Molecular dynamics of ubiquinone inside a lipid bilayer. *J phys chem b* 2001; 105: 9308–9315.

[18] Aranda F, Gomez-Fernandez JC. The interaction of ubiquinone-10 and ubiquinol-10 with phospholipid bilayers. A study using differential scanning calorimetry and turbidity measurements. *Biochim Biophys Acta* 1985; 820: 19–27.

[19] Katsikas H, Quinn PJ. The Distribution of Ubiquinone□10 in Phospholipid Bilayers. *Eur J Biochem* 1982; 124: 165–169.

[20] Ondarroa M, Quinn PJ. A difference infrared-spectroscopic study of the interaction of ubiquinone-10 with phospholipid bilayers. *Biochem J* 1986; 240: 325–331.

[21] Jemiola-Rzeminska M, Kruk J, Skowronek M, et al. Location of ubiquinone homologues in liposome membranes studied by fluorescence anisotropy of diphenyl-hexatriene and trimethylammonium-diphenyl-hexatriene. *Chem Phys Lipids* 1996; 79: 55–63.

[22] Lenaz G, Samorì B, Fato R, et al. Localization and preferred orientations of ubiquinone homologs in model bilayers. *Biochem Cell Biol* 1992; 70: 504–14.

[23] Stidham MA, McIntosh TJ SJ. On the localization of ubiquinone in phosphatidylcholine bilayers. *Biochim Biophys Acta* 1984; 767: 423–431.

[24] Afri M, Ehrenberg B, Talmon Y, et al. Active oxygen chemistry within the liposomal bilayer: Part III: Locating Vitamin E, ubiquinol and ubiquinone and their derivatives in the lipid bilayer. *Chem Phys Lipids* 2004; 131: 107–121.

[25] Samori B, Lenaz G, Battino M, et al. On coenzyme Q orientation in membranes: a linear dichroism study of ubiquinones in a model bilayer. *J Membr Biol* 1992; 128: 193–203.

[26] Quinn PJ, Esfahani MA. Ubiquinones have surface-active properties suited to transport electrons and protons across membranes. *Biochem J* 1980; 185: 715–722.

[27] Nerdal W, Nilsen TRS, Steinkopf S. Coenzyme Q10 localizations in model

membranes. A Langmuir monolayer study. *Biophys Chem* 2015; 207: 74–81.

[28] Quirk A, Lardner MJ, Tun Z, et al. Surface-Enhanced Infrared Spectroscopy and Neutron Reflectivity Studies of Ubiquinone in Hybrid Bilayer Membranes under Potential Control. *Langmuir* 2016; 32: 2225–2235.

[29] Moncelli MR, Becucci L, Nelson a, et al. Electrochemical modeling of electron and proton transfer to ubiquinone-10 in a self-assembled phospholipid monolayer. *Biophys J* 1996; 70: 2716–26.

[30] Hoyo J, Guaus E, Torrent-Burgués J, et al. Electrochemical behaviour of mixed LB films of ubiquinone - DPPC. *J Electroanal Chem* 2012; 669: 6–13.

[31] Tieleman D., Marrink S., Berendsen HJ. A computer perspective of membranes: molecular dynamics studies of lipid bilayer systems. *Biochim Biophys Acta - Rev Biomembr* 1997; 1331: 235–270.

[32] Harb F, Prunetti L, Giudici-Orticoni MT, et al. Insertion and self-diffusion of a monotopic protein, the Aquifex aeolicus sulfide quinone reductase, in supported lipid bilayers. *Eur Phys J E* 2015; 38: 1–11.

[33] Venable RM, Zhang Y, Hardy BJ, et al. Molecular Dynamics Simulations of a lipid bilayer and of hexadecane: An investigation of membrane fluidity. *Science (80-)* 1993; 262: 223–226.

[34] Kruk J, Mysliwa-Kurdziel B, Jemiola-Rzeminska M, et al. Fluorescence lifetimes study of alpha-tocopherol and biological prenylquinols in organic solvents and model membranes. *Photochem Photobiol* 2006; 82: 1309–1314.

[35] Fato R, Battino M, Esposti MD, et al. Determination of Partition and Lateral Diffusion Coefficients of Ubiquinones by Fluorescence Quenching of n-(9-Anthroy1oxy)stearic Acids in Phospholipid Vesicles and Mitochondrial Membranes. *Biochemistry* 1986; 25: 3378–3390.

[36] Marchal D, Boireau W, Laval JM, et al. Electrochemical measurement of lateral diffusion coefficients of ubiquinones and plastoquinones of various isoprenoid chain lengths incorporated in model bilayers. *Biophys J* 1998; 74: 1937–48.

[37] Ulrich EL, Girvin ME, Cramer WA, et al. Location and mobility of ubiquinones of different chain lengths in artificial membrane vesicles. *Biochemistry* 1985; 24: 2501–2508.

[38] Cornell BA, Keniry MA, Post A, et al. Location and activity of ubiquinone 10 and ubiquinone analogues in model and biological membranes. *Biochemistry* 1987; 26: 7702–7707.

[39] Metz G, Howard KP, van Liemt WBS, et al. NMR Studies of Ubiquinone Location in Oriented Model Membranes: Evidence for a Single Motionally-Averaged Population. *J Am Chem Soc* 1995; 117: 564–565.

[40] Ondarroa M, Quinn PJ. Proton magnetic resonance spectroscopic studies of the interaction of ubiquinone-10 with phospholipid model membranes. *Eur J Biochem* 1986; 361: 353–361.

[41] Kingsley PB, Feigenson GW. 1H-NMR study of the location and motion of ubiquinones in perdeuterated phosphatidylcholine bilayers. *Biochim Biophys Acta - Bioenerg* 1981; 635: 602–618.

[42] Salgado J, Villalain J, Gómez-Fernández JC. Magic angle spinning 13C-NMR spin-lattice relaxation study of the location and effects of α-tocopherol, ubiquinone-10 and ubiquinol-10 in unsonicated model membranes. *Eur Biophys J* 1993; 22: 151–155.

[43] Katsikas H, Quinn PJ. The polyisoprenoid chain length influences the interaction of ubiquinones with phospholipid bilayers. *Biochim Biophys Acta - Biomembr* 1982; 689: 363–369.

[44] Roche Y, Peretti P, Bernard S. The redox state influences the interaction of ubiquinones with phospholipid bilayers : A DSC study. *J Therm Anal Calorim* 2007; 89: 867–873.

[45] Hauß T, Dante S, Haines TH, et al. Localization of coenzyme Q10 in the center of a deuterated lipid membrane by neutron diffraction. *Biochim Biophys Acta - Bioenerg* 2005; 1710: 57–62.

[46] Hoyo J, Guaus E, Torrent-Burgués J. Monogalactosyldiacylglycerol and digalactosyldiacylglycerol role, physical states, applications and biomimetic monolayer films. *Eur Phys J E* 2016; 39: 1–11.

[47] Hoyo J, Guaus E, Oncins G, et al. Incorporation of Ubiquinone in supported lipid bilayers on ITO. *J Phys Chem B* 2013; 117: 7498–7506.

[48] Hoyo J, Guaus E, Torrent-Burgués J, et al. Biomimetic monolayer films of digalactosyldiacylglycerol incorporating plastoquinone. *Biochim Biophys Acta - Biomembr* 2015; 1848: 1341–1351.

[49] Jemioła-Rzemińska M, Myliwa-Kurdziel B, Strzałka K. The influence of structure and redox state of prenylquinones on thermotropic phase behaviour of phospholipids in model membranes. *Chem Phys Lipids* 2002; 114: 169–180.

[50] Bilewicz R, Majda M. Monomolecular Langmuir-Blodgett films at electrodes. Formation of passivating monolayers and incorporation of electroactive reagents.

Langmuir 1991; 7: 2794–2802.

[51] Kruk J, Strzałka K, Leblanc RM. Monolayer study of plastoquinones, tocopherol quinone, their hydroquinone forms and their interaction with monogalactosyldiacylglycerol. Charge-transfer complexes in a mixed monolayer. *Biochim Biophys Acta - Biomembr* 1992; 1112: 19–26.

[52] Vitovič P, Nikolelis DP, Hianik T. Study of calix[4]resorcinarene-dopamine complexation in mixed phospholipid monolayers formed at the air-water interface. *Biochim Biophys Acta - Biomembr* 2006; 1758: 1852–1861.

[53] Gzyl-Malcher B, Filek M, Makyła K, et al. Differences in surface behaviour of galactolipoids originating from different kind of wheat tissue cultivated in vitro. *Chem Phys Lipids* 2008; 155: 24–30.

[54] Zhao L, Feng SS. Effects of lipid chain length on molecular interactions between paclitaxel and phospholipid within model biomembranes. *J Colloid Interface Sci* 2004; 274: 55–68.

[55] Roche Y, Peretti P, Bernard S. Influence of the chain length of ubiquinones on their interaction with DPPC in mixed monolayers. *Biochim Biophys Acta - Biomembr* 2006; 1758: 468–478.

[56] Hoyo J, Guaus E, Torrent-Burgués J, et al. Electrochemistry of LB films of mixed MGDG: UQ on ITO. *Bioelectrochemistry* 2015; 104: 26–34.

[57] Mårtensson C, Agmo Hernández V. Ubiquinone-10 in gold-immobilized lipid membrane structures acts as a sensor for acetylcholine and other tetraalkylammonium cations. *Bioelectrochemistry* 2012; 88: 171–180.

[58] Hong HG, Park W. Electrochemical characteristics of hydroquinone-terminated self-assembled monolayers on gold. *Langmuir* 2001; 17: 2485–2492.

[59] Aranda F, Gomez-Fernandez JC. Influence of membrane fluidity on transport mediated ubiquinones through phospholipid vesicles. *Biochem Biophys* 1982; 218: 525–530.